

Testing cosmological models with isotropic and anisotropic components of BAO data

Balakrishna S. Haridasu¹, Vladimir V. Luković^{2,3}, and Nicola Vittorio^{2,3}

¹ Gran Sasso Science Institute, Viale Francesco Crispi 7, I-67100 L'Aquila, Italy

² Dipartimento di Fisica, Università di Roma "Tor Vergata", Via della Ricerca Scientifica 1, I-00133, Roma, Italy

³ Sezione INFN, Università di Roma "Tor Vergata", Via della Ricerca Scientifica 1, I-00133, Roma, Italy

Received / Accepted

ABSTRACT

We conduct a selective analysis of the isotropic (D_V) and anisotropic (AP) components of the Baryon Acoustic Oscillations (BAO) data. We find that these components provide significantly different constraints and could provide strong diagnostics for model selection, also in view of more precise data to arrive. We complemented the BAO data with the Supernova Ia (SNIa) and Observational *Hubble* datasets to perform a joint analysis on the Λ CDM model and its standard extensions. From this analysis, we find a value of $H_0 = 69.4 \pm 1.7$ Km/s Mpc⁻¹ in the Λ CDM scenario, which is now consistent with both the Planck and the direct estimates of Riess et al. We also comment on the possible bias on H_0 estimates introduced by approximate formulae for the sound horizon at drag epoch (r_d). We find that the evidence for acceleration using the BAO data alone is more than $\sim 5.8\sigma$, which increases to 8.4σ in our joint analysis. Using the BAO data alone, we find a 2.2σ deviation from the concordance model in a two-parameter extension of Λ CDM, where both Ω_k and w are considered as free parameters, leaving space for new physics.

Key words. Cosmology: cosmological parameters, dark energy, observations

1. Introduction

The Supernova (SNIa) compilation has so far provided the best observational constraints on the cosmological models for the late-time acceleration. At low-redshifts ($z \lesssim 2$), the SNIa (Betoule et al. 2014) constraints were very well complemented by the Observational Hubble parameter (OHD) (Simon et al. 2005; Moresco et al. 2016; Moresco et al. 2012b) and the Baryon Acoustic Oscillations (BAO) (Eisenstein et al. 2005; Alam et al. 2016).

Cosmological constraints from these low-redshift data are in good agreement with those derived from the very precise high-redshift observations of Cosmic Microwave Background (CMB) (Ade et al. 2016). As a result, the Λ CDM model has emerged as the “concordance model” (Aubourg et al. 2015; Farooq et al. 2017; Wang et al. 2017a). However, several questions have been raised regarding a concordance value for the H_0 (Luković et al. 2016; Bernal et al. 2016). It has been shown time and again that the H_0 value from the direct estimate has been in a possible tension with the indirect model-dependent estimate. The more recent direct estimate Riess et al. (2016) provides $H_0 = (73.24 \pm 1.74)$ Km/s Mpc⁻¹ (hereafter R16), while the Planck collaboration derived $H_0 = (67.31 \pm 0.96)$ Km/s Mpc⁻¹ (Ade et al. 2016). Addison et al. (2017) have estimated an even lower value, $H_0 = 66.98 \pm 1.18$ Km/s Mpc⁻¹, by including the primordial deuterium abundance to the other datasets.

Alongside the tension in the value of H_0 , the current accelerated state of the Universe has also been questioned in Nielsen et al. (2016), which led to a discussion regarding the SNIa analysis and the evidence for a late-time acceleration in Rubin & Hayden (2016); Haridasu et al. (2017); Tutusaus et al. (2017); Dam

et al. (2017). More recently, the BAO dataset has been further improved, owing to the precise measurements from the SDSS (DR12) galaxy survey. Alam et al. (2016) were able to disentangle the degeneracies in the transverse and the radial components in the redshift range $0.35 < z < 0.7$, providing both the transverse comoving distance [$D_M(z)$] and Hubble parameter [$H(z)$]. With this improvement, the current BAO data give the stronger constraints among the other low-redshift observations. In fact, using the BAO dataset alone now gives a significant evidence ($\sim 6.5\sigma$) for acceleration (Ata et al. 2017).

The earlier measurements of the BAO data were reported for a volume averaged angular diameter distance $D_V(z)$ (Eisenstein et al. 2005), which is a one-dimensional isotropic measurement and does not have complete information. The missing information is contained in the anisotropic component, usually termed as the Alcock-Pazynski parameter $AP(z)$ (Alcock & Paczyński 1979). These two components carry different information from the same observations. Using only one of them can lead to biased results and hence incorrect inferences, which has been the case when only the isotropic component was available.

In this paper we use both the isotropic and the anisotropic components of the BAO data to set constraints on cosmological parameters, highlighting the differences when using each component individually. We also show the effects of considering the approximate functions for the sound horizon at the drag epoch. We complement the BAO data with SNIa and OHD data to obtain joint constraints and to further comment on the issues of H_0 and acceleration. We test the nature of dark energy, using a joint analysis of the low-redshift data to constrain the concordance model and its extensions.

The paper is organised as follows. In Section 2 the models tested are briefly described. In Section 3 we present the data

Send offprint requests to: sandeep.haridasu@gssi.it

utilised in this paper, together with a brief description of the method. In Section 4 we report the results of our analysis. Finally, in section Section 5 we summarise our findings and discuss our main conclusions.

2. Models

In this section we briefly describe the concordance Λ CDM model and its standard extensions that we test and compare in our analysis. The Friedmann equation with all standard degrees of freedom at low-redshifts is given by,

$$H(z)^2 = H_0^2 \left[\Omega_m(1+z)^3 + \Omega_k(1+z)^2 + \Omega_{DE}f(z) \right], \quad (1)$$

where, H_0 is the present expansion rate, Ω_m , Ω_{DE} and Ω_k are the dimensionless density parameters of matter, dark energy and curvature, respectively. The dimensionless density parameters obey the cosmic sum rule of $\Omega_m + \Omega_{DE} + \Omega_k = 1$. The general functional form $f(z)$ gives the evolution of the DE and can be written as,

$$f(z) = \exp \left(3 \int_0^z \frac{1+w(\xi)}{1+\xi} d\xi \right), \quad (2)$$

where $w(z)$ is the equation of state (EOS) parameter of the dark energy. Here, a constant in redshift EOS parameter is simply represented as w in contrast to $w(z)$. For the flat Λ CDM model, $\Omega_m = 1 - \Omega_{DE}$ and $w = -1$. We test the standard extensions of Λ CDM model, namely the $k\Lambda$ CDM model with the constraint $\Omega_m = 1 - \Omega_\Lambda - \Omega_k$, and the flat w CDM model with w as a free parameter. The second Friedmann equation, $\ddot{a}/a = -4\pi/3G \sum_i \rho_i(1+3w_i)$, gives us insight into the necessary conditions to be satisfied for assessing the dynamics of expansion rate. The criteria for acceleration can be derived as: $\Omega_m \leq \Omega_\Lambda/2$ for $k\Lambda$ CDM and $w \leq -1/(3\Omega_\Lambda)$ for w CDM. We can assess the evidence for acceleration by estimating the confidence level with which the criteria are satisfied. One can derive the deceleration parameter as,

$$q(z) = -a \frac{\ddot{a}}{\dot{a}^2} \equiv (1+z) \frac{H'(z)}{H(z)} - 1. \quad (3)$$

A negative value of the deceleration parameter today, $q(0)$, implies an expanding universe at an accelerated rate. In addition, one can derive $q_0 = q(0) = 3/2\Omega_m - \Omega_\Lambda$ for Λ CDM and $k\Lambda$ CDM models and $q_0 = 1/2(1+3(1-\Omega_m))$ for w CDM model.

We also study two parameter extensions to Λ CDM, namely kw CDM and the w_0w_a CDM. For the kw CDM model both the w and Ω_k are treated as free parameters. The w_0w_a model is given by Taylor expanding the EOS parameter around $a \sim 1$, as prescribed by the so-called CPL parametrisation (Chevallier & Polarski 2001; Linder 2003),

$$w(z) = w_0 + w_a \frac{z}{1+z}. \quad (4)$$

The luminosity distance for all these models can be written as,

$$D_L(z) = (1+z) \frac{c}{H_0 \sqrt{|\Omega_k|}} S \left(\sqrt{|\Omega_k|} H_0 \int_0^z \frac{d\xi}{H(\xi)} \right) \quad (5)$$

where,

$$S(x) \equiv \begin{cases} \sin(x). & \text{for } \Omega_k < 0 \\ x. & \text{for } \Omega_k = 0 \\ \sinh(x). & \text{for } \Omega_k > 0 \end{cases} \quad (6)$$

Article number, page 2 of 9

The theoretical distance modulus is defined as $\mu_{th} = 5 \log[D_L(\text{Mpc})] + 25$. The comoving angular diameter distance $D_M(z)$ is related to $D_L(z)$ as,

$$D_M(z) = D_L(z)/(1+z), \quad (7)$$

which are used in the modelling of BAO data. Alternatively, the other two useful observables in modelling the BAO data are: $D_V(z)/r_d$ (Eisenstein et al. 2005); $AP(z)$ (Alcock & Paczyński 1979). The volume averaged comoving angular diameter distance $D_V(z)$ is given by,

$$D_V(z) = \left[D_M^2(z) \frac{cz}{H(z)} \right]^{1/3} \quad (8)$$

and, r_d is the sound horizon at the drag epoch (z_d).

$$r_d = \int_{z_d}^{\infty} \frac{c_s(z)}{H(z)} dz \quad (9)$$

The Alcock-Pazynski parameter was primarily defined as a test for the cosmological constant in Alcock & Paczyński (1979) and is written as,

$$AP(z) = D_M(z) \frac{H(z)}{c}. \quad (10)$$

One can easily construct the observables $AP(z)$ and $D_V(z)$ if the measurements for $D_M(z)$ and $H(z)$ are available.

3. Data

In this section we describe the data used and the different methods adopted to test models against the data. In this current work we use the low-redshift BAO, OHD, and SNIa data.

3.1. BAO

The BAO data until recently have been presented for the observable $D_V(z)/r_d$ (Eisenstein et al. 2005), owing to the lack of sufficient statistics to distinctly measure $D_M(z)$ and $H(z)$. The $D_V(z)/r_d$ variable has by far been used to constrain cosmological parameters providing good agreement with the SNIa data (Betoule et al. 2014). These constraints improve once a joint analysis is performed (see, e.g., (Luković et al. 2016)).

In this work we utilise the measurements for $D_M(z)/r_d$ and $H(z)r_d$ (hereafter $D_M\&H$) and conduct a selective analysis using the different information that one can obtain using these measurements. In Alam et al. (2016) measurements of $D_M\&H$ (see their Table 8) at three binned redshifts $z = 0.32, 0.57, 0.61$ were reported using the galaxy clustering data from Sloan Digital Sky Survey(SDSS) III. Earlier, Delubac et al. (2015) have presented the observation of the BAO feature at the binned redshift $z = 2.34$ in the flux-correlation of the Lyman- α forest of high-redshift quasars. Finally, the cross-correlation of Lyman- α forest absorption with the quasars has yielded another measurement at $z = 2.36$ in Font-Ribera et al. (2014). These data points have been updated in du Mas des Bourboux et al. (2017) and Bautista et al. (2017), with improvements implemented in their analyses. These new data points are now given at redshifts $z = 2.33$ and $z = 2.4$. Although, other D_V measurements at $z = 0.106, 0.15, 1.52$ (Beutler et al. 2011; Ross et al. 2015; Ata et al. 2017) are available, we do not implement them in our analysis as the AP component at their respective redshifts is unavailable.

In Alam et al. (2016), the results have also been presented in terms of D_V and AP (hereafter $D_V&AP$) parameter space. Also, the covariance between the D_V and AP points is shown to be negligible. As discussed in Alam et al. (2016), the D_V observable corresponds to a (spherical) volume-averaged angular diameter distance, while the AP variable represents an anisotropy parameter. Note that, the $D_V&AP$ can be derived from the $D_M&H$ measurements (see Eq. (8)) and then they are equivalent for cosmological parameter estimation. We construct a jacobian matrix, J , to propagate the covariance from the $D_M&H$ to the isotropic and the anisotropic basis given by $D_V&AP$ (see Eq. (11)).

$$\Sigma_{D_V&AP} = J^T \cdot \Sigma_{D_M&H} \cdot J, \quad (11)$$

where J is defined as the partial derivatives of the final functional form with respect to the initial functional form. Our formalism of constructing the $D_V&AP$ data points converges very well to the covariances presented in Alam et al. (2016). We implement the same formalism to obtain the $D_V&AP$ data points along with their respective correlations for the Lyman- α data points. The correlations between the D_M and H estimates are taken to be 0.377 and 0.369 at $z=2.33$ and $z=2.4$, respectively (du Mas des Bourboux et al. 2017). This formalism can be easily extended also to the earlier Lyman- α measurements or the tomographic BAO data for the 9 redshift bins presented in Zhao et al. (2016); Wang et al. (2017b) (hereafter (9zSDSS)). The constraints obtained from 9zSDSS data were shown to be more stringent than those using 3 redshift data in Wang et al. (2017a).

In Table 1 we show the measurements of these two components at different redshifts that we implement in our analysis. One can easily verify that the information in $D_V&AP$ and $D_M&H$ is equivalent by comparing the constraints obtained using either of them.

Table 1. BAO data in $D_V&AP$ formalism. The reference I corresponds to Alam et al. (2016)¹, which provides both the data and the covariances. We construct the Lyman- α $D_V&AP$ data using the measurements $D_M&H$ from references II (Bautista et al. 2017) and III (du Mas des Bourboux et al. 2017).

z	D_V/r_d	AP	Reference
0.38	9.995 ± 0.111	0.413 ± 0.013	I
0.51	12.700 ± 0.129	0.597 ± 0.017	I
0.61	14.482 ± 0.149	0.741 ± 0.021	I
2.33	31.123 ± 1.087	4.164 ± 0.317	II
2.4	30.206 ± 0.892	3.962 ± 0.288	III

The transformation of the Lyman- α data points to the $D_V&AP$ basis is summarised in Table 2. One can notice the high correlation of the D_V and AP points at their respective redshifts. The correlation is found to be ~ 0.8 and ~ 0.53 at redshifts of 2.33, 2.4, respectively. Given, the high correlation one must always use the full covariance matrix to compare the constraints from $D_M&H$ and $D_V&AP$.

A simple likelihood for the correlated BAO data in Table 1 is implemented as,

$$\mathcal{L}_{\text{BAO}} \propto \exp \left[(Y_{\text{data}} - Y_{\text{th}}) \cdot \Sigma_{\text{BAO}}^{-1} \cdot (Y_{\text{data}} - Y_{\text{th}})^T \right]. \quad (12)$$

where Y_{data} is the data described in Table 1 and the Y_{th} is the theoretical model evaluated at the respective redshifts, while Σ_{BAO}

¹ All values of the mean, dispersion and covariances of $D_V&AP$ and $D_M&H$ observables for the galaxy clustering BAO data are taken from <https://data.sdss.org/sas/dr12/boos/papers/clustering/>.

Table 2. For completeness we show here the total covariance matrix in $D_V&AP$ basis obtained using the jacobian formalism for the two Lyman- α points at $z = 2.33$ and $z = 2.4$.

Measurement	c_{ij}			
$D_V(2.33)$	1.18205	0.	0.25571	0.
$D_V(2.4)$	0.	0.79666	0.	0.14525
$AP(2.33)$	0.25571	0.	0.10061	0.
$AP(2.4)$	0.	0.14525	0.	0.08271

denotes the total covariance matrix of the BAO data. In our current analysis we fit r_d (joint analysis) or $r_d \times H_0$ (hereafter $H_0 r_d$, for BAO data alone) as a free parameters without implementing any approximate functional forms for our main analysis.

The estimation of r_d has for long been based on the approximate fitting formula developed in Eisenstein & Hu (1998) (hereafter E98), where z_d is given as function of Ω_m and $h = H_0/100$,

$$z_d = \frac{1291(\Omega_m h^2)^{0.251}}{1 + 0.659(\Omega_m h^2)^{0.828}} (1 + b_1(\Omega_b h^2)^{b_2}), \quad (13)$$

where

$$b_1 = 0.313(\Omega_m h^2)^{-0.419} (1 + 0.607(\Omega_m h^2)^{0.674}),$$

$$b_2 = 0.238(\Omega_m h^2)^{0.223}. \quad (14)$$

Recently in Aubourg et al. (2015) (hereafter A15), a new functional form for the estimation of r_d has been given as,

$$r_d = 55.154 \frac{\exp(-72.3(\Omega_v h^2 + 6 \times 10^{-4})^2)}{(\Omega_b h^2)^{0.12807} (\Omega_m h^2 - \Omega_v h^2)^{0.25351}} \quad (15)$$

The r_d estimate obtained using the Eisenstein & Hu (1998) fitting formula for the redshift at drag epoch z_d introduces a dependence of H_0 in $H_0 r_d$. Similarly, the approximate functional form for r_d given in Aubourg et al. (2015) clearly introduces a dependence of $\sim H_0^{-0.763}$ in r_d estimate. We choose to not use either of these formulae for our main analysis, as implementing these formalisms introduces an extra degeneracy between the parameters Ω_m and H_0 , while also requiring to assume the baryon content (Ω_b) from the high-redshift CMB data (Ade et al. 2016) or nucleosynthesis (BBN) measurements. However, we use these approximations to compare the results obtained from our main analysis. We assume the value of $\Omega_b h^2 = 0.0217$ (Riemer-Sørensen & Sem Jensen 2017) and the neutrino density as $\Omega_\nu h^2 = 6.42 \times 10^{-4}$ (Ade et al. 2016) when using E98 and A15.

3.2. OHD and SNIa data

The measurements of the expansion rate have been estimated using the differential age method suggested in Jimenez & Loeb (2002), which considers pairs of passively evolving red galaxies at similar redshifts to obtain dz/dt . We use a compilation of 31 uncorrelated data points taken from Simon et al. (2005); Stern et al. (2010); Moresco et al. (2012a); Moresco et al. (2016); Moresco (2015); Zhang et al. (2014); Ratsimbazafy et al. (2017). A similar compilation was also implemented in Farooq et al.

(2017), but also considering the $H(z)$ measurements from BAO data.

The OHD data plays a very important role in the joint analysis as it is the only dataset capable of discerning the degeneracy between the Hubble parameter H_0 and M_B for supernova data, and the degeneracy between H_0 and r_d in case of BAO data. We implement a simple likelihood function assuming all the data are uncorrelated as,

$$\mathcal{L}_{\text{OHD}} \propto \exp \left[-\frac{1}{2} \sum_{i=1}^{31} \left(\frac{H_i - H(z_i)}{\sigma_{H_i}} \right)^2 \right]. \quad (16)$$

where σ_{H_i} is the gaussian error on the measured value of H_i .

We use the JLA supernova compilation, with the standard χ^2 analysis as is elaborated in Betoule et al. (2014). The JLA supernova compilation implements a correction to the absolute magnitude through the empirical relation,

$$M_B^{\text{corr}} = M_B - \alpha s + \beta c, \quad (17)$$

where M_B is the absolute magnitude, s and c are the stretch and colour corrections for the absolute magnitude. The likelihood for the SNIa data has been defined by evaluating an intrinsic scatter of 0.108 through the use of reduced maximum likelihood method (Betoule et al. 2014). The observed distance modulus μ_{obs} can be written as,

$$\mu_{obs} = m_B - M_B^{\text{corr}} + \alpha s - \beta c, \quad (18)$$

The likelihood for the SNIa data can be written as,

$$\mathcal{L}_{\text{SN}} \propto \exp \left[\frac{(\mu_{obs} - \mu_{th})^T \cdot Cov^{-1} \cdot (\mu_{obs} - \mu_{th})}{|Cov|} \right]. \quad (19)$$

where Cov denotes the total covariance matrix including the correction for the host galaxy mass.

Finally, the joint analysis is performed by combining the likelihoods for these independent datasets. The likelihood for the joint analysis is given as,

$$\mathcal{L}_{\text{tot}} = \mathcal{L}_{\text{BAO}} \mathcal{L}_{\text{OHD}} \mathcal{L}_{\text{SN}}. \quad (20)$$

We use the Akaike information criteria (AIC) (Akaike 1974) and Bayesian information (BIC) (Schwarz et al. 1978) for model selection. The AIC and AICc (corrected for number of data points) with a second-order correction term, are written as,

$$\text{AIC} = -2 \log \mathcal{L}^{\text{max}} + 2N_p, \quad (21)$$

$$\text{AICc} = -2 \log \mathcal{L}^{\text{max}} + 2N_p + \frac{2N_p(N_p + 1)}{N_d - N_p - 1}, \quad (22)$$

where N_p is the number of parameters and N_d is the number of data points. For large N_d , the AICc value tends to AIC, while for less N_d (for example: BAO data) it penalises the model with more parameters strongly. Similarly the BIC can be defined as,

$$\text{BIC} = -2 \log \mathcal{L}^{\text{max}} + N_p \log(N_d), \quad (23)$$

The model preference is estimated by evaluating ΔAICc (ΔBIC) as a difference in the AICc value of the model in question to the reference model. A positive value of ΔAICc or ΔBIC indicates that the reference model is preferred over the model in comparison.

4. Results and Discussion

In this section we present the results obtained from our analysis for BAO data alone and then for the joint analysis described in the earlier sections. We also comment on the strong statistical evidence for a late-time acceleration phase.

4.1. Results from the analysis of BAO data

As mentioned in the earlier sections we have used the different observables (D_V , AP , $D_V \& AP$ and $D_M \& H$) taken from the BAO data to constrain the standard model and its extensions. In Table 3, Table 4 and Table 5 we show the best-fit parameters to ΛCDM , $k\Lambda\text{CDM}$ and $w\text{CDM}$ models using each of the four observables. The AP measurements give a high value of Ω_Λ for all the standard extensions considered, while the D_V measurements give lower values of the same with very similar power to constrain the mean value. However, in the $k\Lambda\text{CDM}$ model we find that using AP only results in unexpected high values of Ω_m and Ω_Λ (see lower panel of Figure 1). The Ω_m estimates obtained using the D_V and AP components separately for ΛCDM model show a mild disagreement² of 2.1σ . When the 9zSDSS data is used this discrepancy is even more and they agree only at 3.3σ . As expected, we find that using the BAO data in either the $D_M \& H$ or $D_V \& AP$ formalism yields very consistent results suggesting that there is no loss of information and that these two parameter spaces are equivalent (see Figure 1). In Addison et al. (2017), the authors have done an extended analysis by splitting the data into $D_M(z)$ and $H(z)$ components, and comparing the $D_M \& H$ with D_V , while not considering AP as we are doing here. They have reported a tension of $\sim 2.4\sigma$ between the ‘‘low-redshift’’ galaxy-clustering BAO data and the older ‘‘high-redshift’’ Lyman- α data. However, we find this tension is now lowered, as the Lyman- α measurements have been revised in Bautista et al. (2017); du Mas des Bourboux et al. (2017) with larger dispersions.

Table 3. Fit parameters to the BAO data in the four different formalisms for ΛCDM model.

Data	Ω_m	$H_0 r_d [\text{Km/s}]$
AP	$0.225^{+0.045}_{-0.040}$	-
D_V	$0.358^{+0.043}_{-0.038}$	9840^{+204}_{-212}
$D_V \& AP$	$0.285^{+0.019}_{-0.017}$	10182 ± 139
$D_M \& H$	$0.288^{+0.019}_{-0.018}$	10162 ± 139

We find that a consistent estimate for the flatness in the $k\Lambda\text{CDM}$ model can only be obtained when both D_V and AP data are used together (see bottom panel of Figure 1). In the $w\text{CDM}$ model, we find that the ability of the AP measurements to constrain the value of w is better than that of D_V measurements. Hence, the inclusion of the AP measurements is crucial to have reliable inferences, e.g., on the phantom scenario (see Figure 2). The ability of the BAO data to constrain the $w_0 w_a \text{CDM}$ and the $k w\text{CDM}$ models will be discussed in the next subsection, alongside the joint analysis.

² Due to the lack of proper formalism to estimate the tension between the parameters obtained using covarying datasets, we quote the tension without using the covariance. If the covariance is also taken into account the estimated tension is only bound to increase.

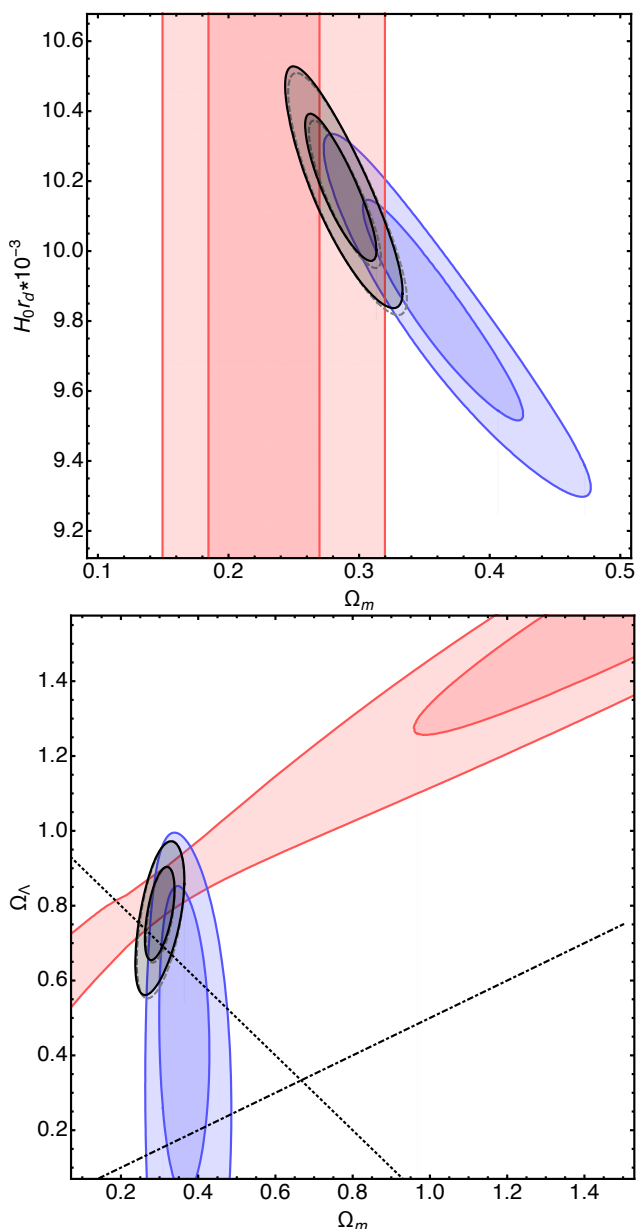


Fig. 1. The red, blue and black contours correspond to AP , D_V and $D_V \& AP$ methods, respectively. We show here the 68% and 95% confidence level contours. The dotted line in the bottom panel correspond to the flat model, the dot-dashed line marks the transition between the accelerated and non-accelerated regimes. The Dashed contours in both the panels shows the constrains using $D_M \& H(z)$ formalism.

So far, in our analysis, we have not utilised any approximate functional form for the r_d estimate. When used, it seems that BAO data alone is able to estimate also the H_0 parameter. We implement the two approximate functional forms E98 and A15 to compare the constraints with those obtained while fitting the $H_0 r_d$ parameter. Although these functional forms allow us to estimate the value of H_0 , it is only a false dependence that is introduced by the approximate formulae. In reality, the BAO data does not have any information about H_0 , as the parameter $H_0 r_d$ is independent of the Hubble constant. In Table 6 we show the values of H_0 obtained by using either of the approximate formulae. While it is appreciable that the estimate of Ω_m is unaltered when using the fitting formulae, the value of H_0 is completely dependent on the approximate formulae and, also, biased. In-

Table 4. Best-fit parameters to the BAO data in the four different formalisms for Λ CDM model.

Data	Ω_m	Ω_Λ	$H_0 r_d$ [Km/s]
AP	$1.748^{+0.561}_{-0.521}$	$1.72^{+0.306}_{-0.301}$	-
D_V	$0.358^{+0.045}_{-0.04}$	$0.537^{+0.224}_{-0.306}$	9632^{+504}_{-550}
$D_V \& AP$	0.3 ± 0.025	$0.786^{+0.079}_{-0.085}$	10303^{+199}_{-199}
$D_M \& H$	0.302 ± 0.024	$0.783^{+0.081}_{-0.087}$	10285 ± 202

Table 5. Best-fit parameters to the BAO data in the four different methods for w CDM model.

Data	Ω_m	w	$H_0 r_d$ [Km/s]
AP	$0.157^{+0.062}_{-0.082}$	$-0.646^{+0.166}_{-0.174}$	-
D_V	$0.353^{+0.046}_{-0.104}$	$-0.822^{+0.387}_{-0.443}$	9570^{+727}_{-551}
$D_V \& AP$	$0.275^{+0.023}_{-0.035}$	$-0.736^{+0.166}_{-0.169}$	9692^{+334}_{-304}
$D_M \& H$	$0.278^{+0.024}_{-0.036}$	$-0.741^{+0.171}_{-0.174}$	9690^{+340}_{-308}

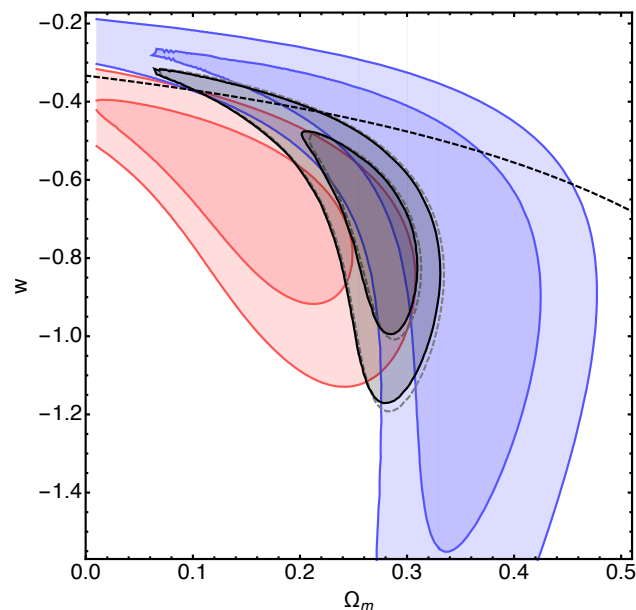


Fig. 2. The red, blue and black contours correspond to AP , D_V and $D_V \& AP$ methods, respectively. We show here the 68% and 95% confidence level contours. The Dashed contours in grey show the constrains using $D_M \& H(z)$ method. The region below (above) the dashed line corresponds to the accelerating (non-accelerating) regime.

terestingly, the value of $H_0 = 67.35^{+2.03}_{-1.81}$ is consistent with the CMB estimate when using the $D_V(z)$ data alone with E98. On the contrary, using A15 and $D_V(z)$ data yields a higher value of $H_0 = 70.42^{+1.66}_{-1.70}$, closer to the Riess et al. (2016) result. Inclusion of other three BAO D_V -only points at $z = 0.106, 0.15, 1.52$ affects the constraints from the BAO data mildly. For instance, in the Λ CDM model we obtain $\Omega_m = 0.293^{+0.18}_{-0.17}$, showing clearly the minimal effect that these data have on constraining the model. We then proceed with the joint analysis not including these three data points.

Table 6. Comparison of H_0 estimates from $D_M&H$ data alone, while implementing different approximate formulae for Λ CDM model.

Data	Ω_m	H_0 Km/s Mpc $^{-1}$
$D_M&H$ +E98	$0.288^{+0.019}_{-0.018}$	$64.11^{+1.04}_{-1.00}$
$D_M&H$ +A15	$0.288^{+0.019}_{-0.018}$	67.18 ± 1.15

4.2. Joint analysis and model selection

In this section we discuss the constraints obtained from the joint analysis of $D_M&H$ +SN+OHD data. We show that the BAO data are now driving these constraints, as it is the more precise dataset among the other “low-redshift” data. In table 7 we show our findings. The estimates for H_0 are consistent among all the models considered here. Note the low value of Ω_m obtained for the w_0w_a CDM model.

Table 7. Best-fit estimates and parameter constraints using the $D_M&H$ +SN+OHD data.

Model	Ω_m	H_0	w_0/w	w_a	Ω_Λ
Λ CDM	$0.292^{+0.016}_{-0.015}$	69.41 ± 1.76	-	-	-
$k\Lambda$ CDM	0.296 ± 0.024	$69.62^{+2.2}_{-1.98}$	-	-	$0.722^{+0.064}_{-0.067}$
w CDM	0.285 ± 0.018	$68.61^{+1.93}_{-1.91}$	$-0.921^{+0.08}_{-0.081}$	-	-
w_0w_a CDM	$0.195^{+0.084}_{-0.23}$	$68.75^{+1.95}_{-1.92}$	$-0.902^{+0.222}_{-0.125}$	$0.838^{+0.217}_{-0.655}$	-
kw CDM	0.311 ± 0.025	$69.27^{+2.0}_{-1.97}$	$-0.828^{+0.075}_{-0.089}$	-	0.872 ± 0.107

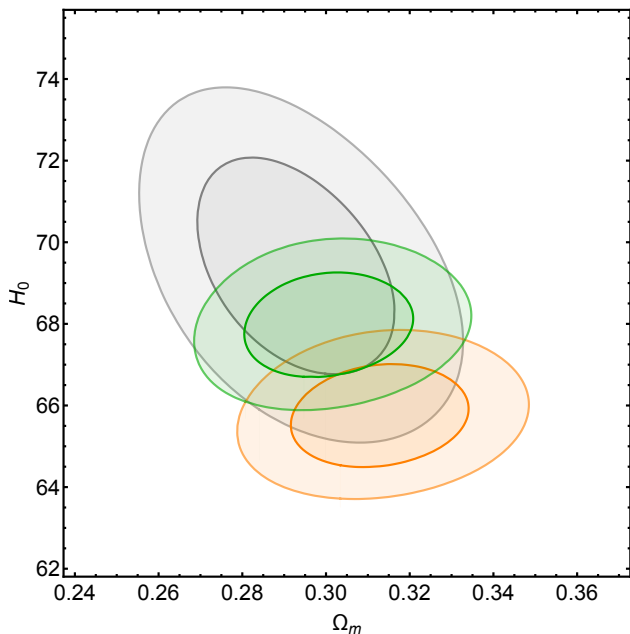


Fig. 3. The Grey contours correspond to $D_M&H$ +SN+OHD data, while the orange contours is given by $D_M&H$ +SN+OHD+E98 and the purple contours by $D_M&H$ +SN+OHD+A15. We show here the 68% and 95% confidence level contours. All contours are made for the Λ CDM model.

In Figure 3 we show the effect of using the approximate formulae in the joint analysis. The E98 and A15 formulae drive the combined analysis towards higher values of Ω_m . As expected,

they provide tighter constraints on H_0 , but with an altered correlation between Ω_m and H_0 . Among all the datasets considered here, OHD is the only dataset capable of providing a constraint on H_0 . Implementing the approximate formulae with data that do not already have the ability to constrain H_0 can lead to biased results. We find very consistent estimates for the r_d , which we do not explicitly quote in Table 7, for instance in the Λ CDM model our best-fit value is $r_d = 146.03^{+3.59}_{-3.43}$.

We find the best-fit estimate of H_0 for the Λ CDM model to be $H_0 = 69.41 \pm 1.76$ Km/s Mpc $^{-1}$. Note that this value is now in the middle of the Planck Collaboration et al. (2016) ($H_0 = 66.93 \pm 0.62$) and the R16 ($H_0 = 73.24 \pm 1.74$) estimates, and consistent with both at 1.33σ and 1.55σ , respectively. A 12-parameter extended CMB analysis in Di Valentino et al. (2016) has shown to reconcile the direct and indirect H_0 estimates. However, their constraint on $w = -1.29^{+0.15}_{-0.12}$ using CMB data and R16 prior is in a $\sim 2.2\sigma$ tension with $w = -0.92 \pm 0.08$ from our joint analysis. In Wang et al. (2017a), the authors have used the E98 formula along BAO data to quote $H_0 = 71.75 \pm 3.05$. Although in agreement with Planck Collaboration et al. (2016), R16 and our joint analysis estimates, this result is due to the use of E98. In addition, we note that the inclusion of the three D_V -only points by itself drives H_0 to slightly higher values. In a more recent work (DES Collaboration et al. (2017)), a combination of five independent datasets namely, CMB+DES+BAO+BBN+(SPTpol Henning et al. (2017)) along with constraints from Sh0ES (Riess et al. 2016) and H0LiCOW (Bonvin et al. 2017) was implemented to quote a value of $H_0 = 69.1^{+0.4}_{-0.6}$, which we are in a very good agreement with.

We find that an assumption of any approximate formula (E98, A15) in the w_0w_a CDM model tends to improve the agreement with the standard model, while in the kw CDM model the approximate formulae do not show any significant influence on the constraints from joint analysis. However, the kw CDM model is in agreement with the standard model at 1.12σ from our joint analysis, while using $D_M&H$ data alone shows that the standard model is in agreement only at 2.2σ (see Figure 4). The individual priors of $\Omega_k = 0$ in the w CDM model and $w = -1$ in $k\Lambda$ CDM model tend to converge their model constraints to Λ CDM. While, leaving both parameters free shows a marginal deviation from Λ CDM.

In Di Valentino et al. (2017) a 12 parameter extended analysis of CMB data along with the BAO and SN data was used to claim a $\sim 2\sigma$ deviation from the standard model. Complementary results were also presented in Joudaki et al. (2017) using joint analysis of CMB and weak lensing data. These results suggest to exclude the first quadrant ($w_0 > -1, w_a > 0$) at $\gtrsim 2\sigma$ confidence. On the contrary, the constraints for the w_0w_a CDM model obtained from our joint analysis tend towards the first quadrant and the standard model is consistent only at 1σ (see Figure 5). Our results are not in immediate agreement with the previous results, which is due to the strong influence of the CMB data that seems to favour phantom scenario (Ade et al. 2016). Similar observations were also made in Bernal et al. (2016) and Di Valentino et al. (2017) using an older compilation of BAO dataset. These results do not seem to change even with the newer BAO dataset that is implemented in the current work.

The CPL parametrisation was shown to be a very good approximation for a wide range of scalar field models and modified gravity scenarios in Linder (2015). However, taking into account the discrepant results from the BAO and the CMB data one could infer that the CPL parametrisation is unable to provide conclusive evidence for dynamical nature of dark energy. This evidence should be more generally inferred for a physically motivated

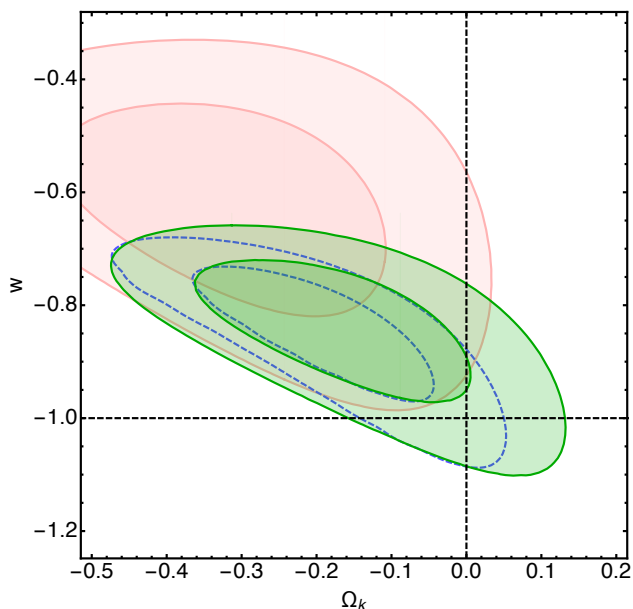


Fig. 4. Here we show the 68% and 95% confidence level contours obtained for the $k\omega$ CDM model using $D_M&H(z)+SN+OHD$ data, with (blue) and without (green) the approximate formula A15. The intersection of the dashed lines $(-1, 0)$ correspond to the standard model. The red contours correspond to the $k\omega$ CDM fit using the $D_M&H$ data alone.

$w(z)$ or through a model independent analysis instead of a simple Taylor expansion around $a = 1$, which is imposed over the range of data $0.285 < a < 1$. In fact, Zhao et al. (2017) predicted an oscillatory nature for dark energy EOS using model-independent technique. They have quoted a 3.5σ preference for this dynamical dark energy over Λ CDM using the Kullback-Leibler divergence, which the bayesian evidence is unable to provide. In fact, we find that w_0w_a CDM is disfavoured over Λ CDM with $\Delta BIC = 10.9$. The standard information criteria like BIC tend to heavily penalise models with extra parameters as the number of data points increase.

In Table 8 we show the values of the information criteria obtained from the joint analysis and $D_M&H$ data alone for the four models tested against Λ CDM. $\Delta AICc$ strongly disfavour the extended models for $D_M&H$ data alone, while ΔBIC strongly penalises them in the joint analysis.

Table 8. Comparison of the $\Delta AICc$ and ΔBIC criteria for the extended models with Λ CDM as the reference model. The first two columns correspond to the joint analysis and the last two columns are estimated from $D_M&H$ data alone.

Model	$\Delta AICc$	ΔBIC	$\Delta AICc_{D_M&H}$	$\Delta BIC_{D_M&H}$
w CDM	1.09	5.71	2.15	0.16
$k\Lambda$ CDM	1.20	6.61	3.58	1.60
$k\omega$ CDM	0.97	10.20	3.05	-2.63
w_0w_a CDM	1.67	10.90	7.42	1.74

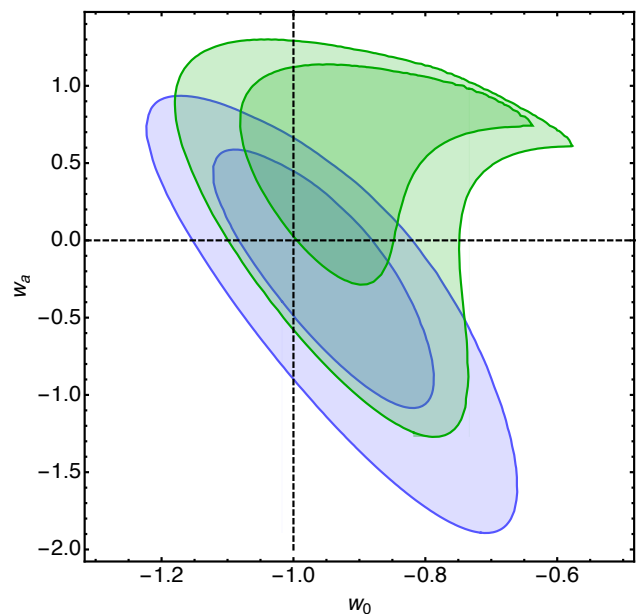


Fig. 5. Here we show the 68% and 95% confidence level contours obtained for the w_0w_a CDM model using $D_M&H(z)+SN+OHD$ data, with (blue) and without (green) the approximate formula A15. The intersection of the dashed lines $(-1, 0)$ correspond to the standard model.

4.3. Comment on acceleration

SNIa observations have been the first to provide an evidence for acceleration (Riess et al. 1998; Perlmutter et al. 1999). In more recent work this evidence has been questioned Nielsen et al. (2016) and further discussed (Rubin & Hayden 2016; Haridasu et al. 2017; Tutusaus et al. 2017; Dam et al. 2017). However, the recent BAO data is now capable of constraining the acceleration with much higher significance. In an earlier work, Ata et al. (2017) have quoted an evidence of 6.5σ using the BAO data alone. In the $k\Lambda$ CDM scenario, using the $D_M&H$ data, we find, in agreement with Ata et al. (2017), that the acceleration is significant at 5.8σ . It is important to note that the evidence for acceleration obtained using the BAO data is coming from the AP component. In fact, using AP alone we find that acceleration is preferred at 6.0σ . On the contrary, the D_V component is incapable of constraining the acceleration, while it constrains Ω_m extremely well (see bottom panel of Figure 1). The evidence for the late-time acceleration increases when a joint analysis is performed: in the $k\Lambda$ CDM scenario, we obtain a significance of 8.5σ . On the other hand, BAO data unlike SNIa is unable to provide a significant evidence for acceleration in the w CDM model (see Figure 2).

In Figure 6 we show the $H_0 - q_0$ plane, where the significance of acceleration and the H_0 estimates can be compared simultaneously. We find that all the models predict very consistent H_0 and q_0 values, while w CDM model shows the least evidence for an accelerated scenario. In Feeney et al. (2017), the direct estimate of H_0 has been reevaluated with various effects of varying distributions and variation in q_0 parameter being taken into account. It was shown that the direct estimate is unaltered under several considerations and they quote a value of $H_0 = 72.72 \pm 1.67$ (without including the SNIa outliers). The model-dependent (Λ CDM) H_0 estimates coming from “high-redshift” CMB and our “low-redshift” joint analysis differ from the model-independent direct measurement of R16. The three estimates of the Hubble constant are in a total tension of 3.9σ . Given that, it seems less likely to resolve the H_0 problem without considering new physics.

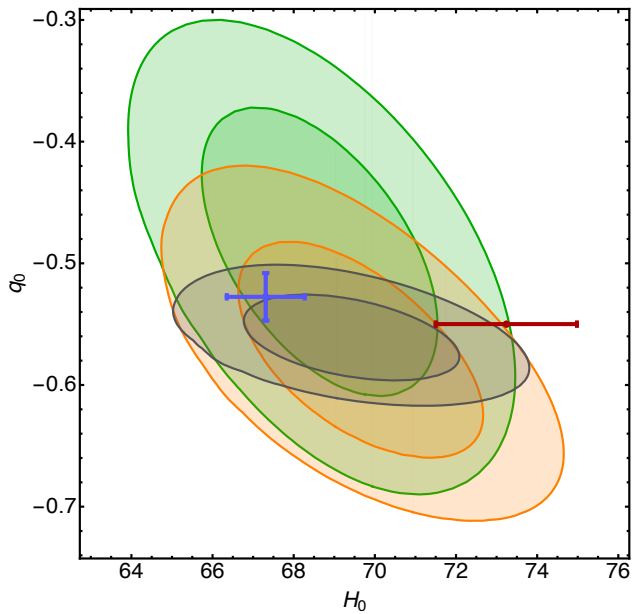


Fig. 6. Here we show the q_0 vs H_0 plots for three different models. The green, orange and grey contours are shown for w CDM, $k\Lambda$ CDM and Λ CDM, respectively. All contours are made using $D_M&H$ +SN+OHD. In blue we show the Planck constraints and Riess H_0 in red.

4.4. Analysis on mock data

We implement a mock dataset with Euclid-like (see Table VI. of Font-Ribera et al. (2013)) precision built around our best-fit k_w CDM model ($\Omega_m = 0.3$, $\Omega_\Lambda = 1.0$, $w = -0.6$, $H_0 r_d = 9610$) obtained using $D_M&H$ data alone. We fit the AP and D_V components of the mock data separately to emphasise the role of their disagreement for model selection. When we fit these two components to Λ CDM model, the corresponding values of Ω_m are in a strong tension, at 6.4σ (see top panel of Figure 7). Likewise, fitting $k\Lambda$ CDM model also shows a strong disagreement as can be seen in the middle panel of Figure 7. As expected, once we use the k_w CDM model, we find a good agreement in the constraints obtained from the AP and D_V components both of which contain the “true” model (see bottom panel of Figure 7). Note, that the w parameter is better constrained by AP rather than by D_V .

The ability of the AP and D_V data to provide model selection can also be complemented by the standard information criteria for model selection. In fact, the latter indicates a clear preference for the “true” model (see Table 9). However, when the “true” model is unknown, even an insignificant evidence for model selection based on standard information criteria can be increased by comparing the AP and D_V constraints. For example, according to standard information criteria, w CDM and $w_0 w_a$ CDM models perform as well as Λ CDM, even if none of them is the “true” model. The $k\Lambda$ CDM model is clearly preferred over the previous three models with $\Delta BIC \sim 50$. However, the middle panel shows that the AP and D_V strongly disagree. Finally, the k_w CDM is performing better than $k\Lambda$ CDM, both using the $\Delta BIC \sim 15$, and AP and D_V . So, an inspection of the D_V and AP constraints can provide a very useful guideline for model selection, as both these components are obtained from same dataset and do not have different systematics.

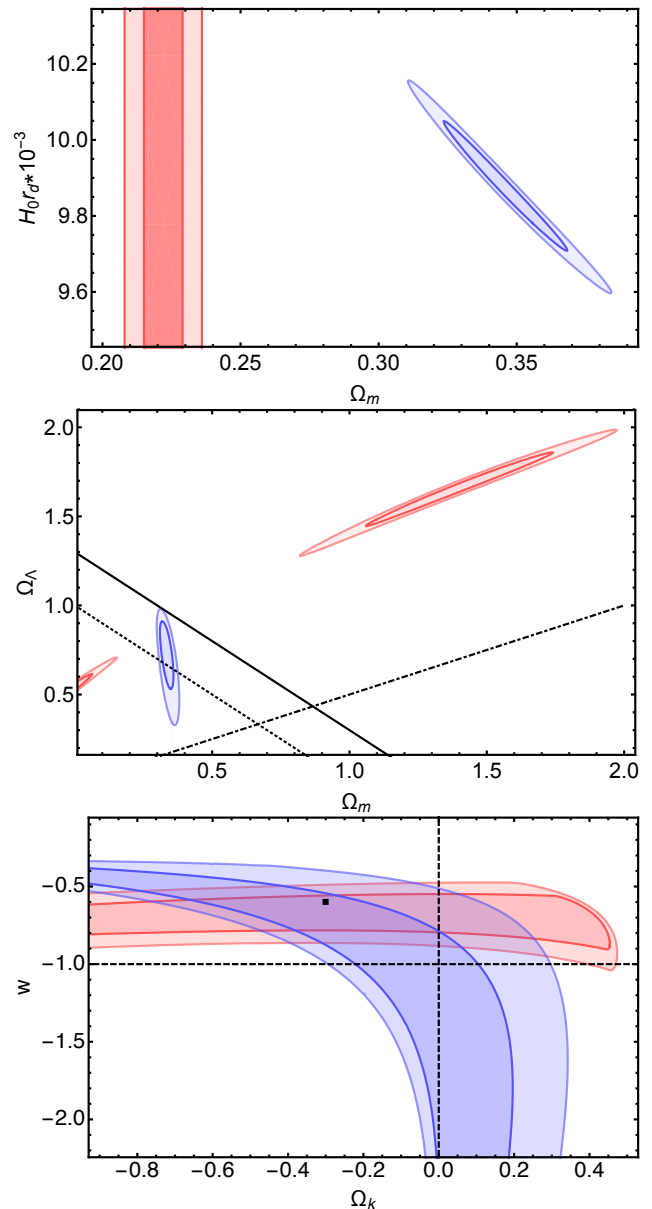


Fig. 7. In the upper panel we show the constraints obtained for the Λ CDM model from our mock dataset using the D_V (blue) and the AP (red) components separately. Similarly, we show the constraints in $k\Lambda$ CDM (middle panel) and k_w CDM (lower panel) scenario. The solid line in the middle panel corresponds to curvature of the model of the mock dataset ($\Omega_k = -0.3$). The dotted line in the middle panel correspond to the flat model, the dot-dashed line marks the transition between the accelerated and non-accelerated regimes. In bottom panel the square marks the “true” model around which the mock data has been constructed and the dashed lines show the standard model.

5. Conclusions

In this work we have explored how different components of the BAO data constrain cosmological parameters. We find that the isotropic D_V and the anisotropic AP components can provide different constraints when used separately. We find a mild tension of 2.1σ for the Ω_m values estimated in the Λ CDM scenario, which increases to 3.3σ when the 9zSDSS data is used. Although, the current discrepancies are not very significant, similar comparison can be utilised to falsify cosmological models with more precise data to come from future experiments such as EUCLID (Laureijs et al. 2011) and DESI (Collaboration et al.

Table 9. Comparison of the ΔAICc and ΔBIC criteria for the extended models with ΛCDM as the reference model. The first two columns correspond to the joint analysis and the last two columns are estimated from $D_M&H$ data alone.

Model	$\Delta\text{AICc}_{D_M&H}$	$\Delta\text{BIC}_{D_M&H}$
$w\text{CDM}$	0.68	1.60
$k\Lambda\text{CDM}$	-55.10	-54.17
$kw\text{CDM}$	-69.42	-67.77
$w_0w_d\text{CDM}$	2.70	4.34

2016a,b). Such a method could be utilised to circumvent the problem of possible systematics in the data.

From our joint analysis, we find $H_0 = 69.41 \pm 1.76$, which is now consistent with both Planck and R16 at 1.33σ and 1.55σ , respectively. Our findings also very well agree with the most stringent constraint of $69.1^{+0.4}_{-0.6}$ quoted in DES Collaboration et al. (2017). However, in the ΛCDM scenario, the three H_0 estimates -from this work, Planck and R16- now have a total tension of 3.9σ , increasing the difficulty to have a concordance value for H_0 . We have also shown that, in the BAO analysis, the use of an assumed approximate formula for r_d to estimate H_0 could lead to biased results.

Using BAO data in the D_V formalism alone can give rise to strict constraints on Ω_m , but not on the cosmic dynamics. This could give the impression that the BAO data is incapable of constraining acceleration. On the contrary, AP provides strong constraints on the acceleration. In fact, the evidence for acceleration is now very strong, at $\sim 5.8\sigma$ from the BAO data alone, and re-confirms the findings from the SNIa data. Using SNIa, OHD and BAO data this evidence is found to be 8.4σ .

In the $kw\text{CDM}$ scenario, using $D_M&H$ data alone, we find a mild deviation of 2.2σ from the standard model. Using the CPL parameterisation we find no evidence for dynamical nature of dark energy from our joint analysis. Although, the BAO data is now providing much better constraints, the dynamical nature of dark energy still eludes in the standard methods for model selection. We also present a mock scenario in which we show how our conclusions can be useful to derive significant inferences from future data.

References

- Addison, G. E., Watts, D. J., Bennett, C. L., et al. 2017, ArXiv e-prints [arXiv:1707.06547]
- Ade, P., Aghanim, N., Arnaud, M., et al. 2016, A&A, 594, A13
- Akaike, H. 1974, IEEE Transactions on Automatic Control, 19, 716
- Alam, S., Ata, M., Bailey, S., et al. 2016, arXiv preprint arXiv:1607.03155
- Alcock, C. & Paczyński, B. 1979, Nature, 281, 358
- Ata, M., Baumgarten, F., Bautista, J., et al. 2017, ArXiv e-prints [arXiv:1705.06373]
- Aubourg, É., Bailey, S., Bautista, J. E., et al. 2015, Phys. Rev. D, 92, 123516
- Delubac, T., Bautista, J. E., Busca, N. G., et al. 2017, A&A, 603, A12
- Bernal, J. L., Verde, L., & Riess, A. G. 2016, J. Cosmology Astropart. Phys., 2016, 019
- Betoule, M., Kessler, R., Guy, J., et al. 2014, A&A, 568, A22
- Beutler, F., Blake, C., Colless, M., et al. 2011, MNRAS, 416, 3017
- Bonvin, V., Courbin, F., Suyu, S. H., et al. 2017, MNRAS, 465, 4914
- Chevallier, M. & Polarski, D. 2001, International Journal of Modern Physics D, 10, 213
- Collaboration, D., Aghamousa, A., Aguilar, J., et al. 2016a, ArXiv e-prints [arXiv:1611.00036]
- Collaboration, D., Aghamousa, A., Aguilar, J., et al. 2016b, ArXiv e-prints [arXiv:1611.00037]
- Dam, L. H., Heinesen, A., & Wiltshire, D. L. 2017, MNRAS, 472, 835
- Delubac, T., Bautista, J. E., Busca, N. G., et al. 2015, A&A, 574, A59
- DES Collaboration, Abbott, T. M. C., Abdalla, F. B., et al. 2017, ArXiv e-prints [1711.00403v1]
- Di Valentino, E., Melchiorri, A., Linder, E. V., & Silk, J. 2017, Phys. Rev. D, 96, 023523
- Di Valentino, E., Melchiorri, A., & Silk, J. 2016, Physics Letters B, 761, 242
- du Mas des Bourboux, H., Goff, J.-M. L., Blomqvist, M., et al. 2017 [1708.0225v1]
- Eisenstein, D. J. & Hu, W. 1998, ApJ, 496, 605
- Eisenstein, D. J., Zehavi, I., Hogg, D. W., et al. 2005, ApJ, 633, 560
- Farooq, O., Madiyar, F. R., Crandall, S., & Ratra, B. 2017, ApJ, 835, 26
- Feeney, S. M., Mortlock, D. J., & Dalmaso, N. 2017, ArXiv e-prints [arXiv:1707.00007]
- Font-Ribera, A., Kirkby, D., Busca, N., et al. 2014, J. Cosmology Astropart. Phys., 5, 27
- Font-Ribera, A., McDonald, P., Mostek, N., et al. 2013, ArXiv e-prints [1308.4164v2]
- Haridasu, B. S., Luković, V. V., D'Agostino, R., & Vittorio, N. 2017, A&A, 600, L1
- Henning, J. W., Sayre, J. T., Reichardt, C. L., et al. 2017, ArXiv e-prints [1707.09353v2]
- Jimenez, R. & Loeb, A. 2002, ApJ, 573, 37
- Joudaki, S., Mead, A., Blake, C., et al. 2017, MNRAS, 471, 1259
- Laureijs, R., Amiaux, J., Arduini, S., et al. 2011, ArXiv e-prints [arXiv:1110.3193]
- Linder, E. V. 2003, Physical Review Letters, 90, 091301
- Linder, E. V. 2015 [1501.01634v1]
- Luković, V. V., D'Agostino, R., & Vittorio, N. 2016, A&A, 595, A109
- Moresco, M. 2015, MNRAS, 450, L16
- Moresco, M., Cimatti, A., Jimenez, R., et al. 2012a, J. Cosmology Astropart. Phys., 8, 006
- Moresco, M., Pozzetti, L., Cimatti, A., et al. 2016, J. Cosmology Astropart. Phys.[1601.01701v2]
- Moresco, M., Verde, L., Pozzetti, L., Jimenez, R., & Cimatti, A. 2012b, J. Cosmology Astropart. Phys., 7, 053
- Nielsen, J. T., Guffanti, A., & Sarkar, S. 2016, Scientific Reports, 6, 35596
- Perlmutter, S., Aldering, G., Goldhaber, G., et al. 1999, ApJ, 517, 565
- Planck Collaboration, Aghanim, N., Ashdown, M., et al. 2016, A&A, 596, A107
- Ratsimbazafy, A. L., Loubser, S. I., Crawford, S. M., et al. 2017, MNRAS, 467, 3239
- Riemer-Sørensen, S. & Sem Jensen, E. 2017, ArXiv e-prints [arXiv:1705.03653]
- Riess, A. G., Filippenko, A. V., Challis, P., et al. 1998, AJ, 116, 1009
- Riess, A. G., Macri, L. M., Hoffmann, S. L., et al. 2016, ApJ, 826, 56
- Ross, A. J., Samushia, L., Howlett, C., et al. 2015, MNRAS, 449, 835
- Rubin, D. & Hayden, B. 2016, ApJ, 833, L30
- Schwarz, G. et al. 1978, The annals of statistics, 6, 461
- Simon, J., Verde, L., & Jimenez, R. 2005, Phys. Rev. D, 71, 123001
- Stern, D., Jimenez, R., Verde, L., Stanford, S. A., & Kamionkowski, M. 2010, ApJS, 188, 280
- Tutusaus, I., Lamine, B., Dupays, A., & Blanchard, A. 2017, A&A, 602, A73
- Wang, Y., Xu, L., & Zhao, G.-B. 2017a, ArXiv e-prints [arXiv:1706.09149]
- Wang, Y., Zhao, G.-B., Chuang, C.-H., et al. 2017b, Monthly Notices of the Royal Astronomical Society, 469, 3762
- Zhang, C., Zhang, H., Yuan, S., et al. 2014, Research in Astronomy and Astrophysics, 14, 1221
- Zhao, G.-B., Raveri, M., Pogosian, L., et al. 2017, Nature Astronomy, 1, 627
- Zhao, G.-B., Wang, Y., Saito, S., et al. 2016, Monthly Notices of the Royal Astronomical Society, 466, 762